

Keyvan Amini Khoiy

Department of Biomedical Engineering,
The University of Akron,
Akron, OH 44325
e-mail: ka67@ziips.uakron.edu

Dipankar Biswas

Department of Mechanical Engineering,
The University of Akron,
Akron, OH 44325
e-mail: db76@ziips.uakron.edu

Thomas N. Decker

Department of Biomedical Engineering,
The University of Akron,
Akron, OH 44325
e-mail: tnd14@ziips.uakron.edu

Kouros T. Asgarian

Cardiothoracic Surgery,
St. Joseph's Regional Medical Center,
Paterson, NJ 07503
e-mail: ktacardiac@aol.com

Francis Loth

Department of Mechanical Engineering,
The University of Akron,
Akron, OH 44325
e-mail: loth@uakron.edu

Rouzbeh Amini¹

Mem. ASME
Department of Biomedical Engineering,
The University of Akron,
260 S Forge Street,
Olson Research Center Room 301F,
Akron, OH 44325
e-mail: ramini@uakron.edu

Surface Strains of Porcine Tricuspid Valve Septal Leaflets Measured in Ex Vivo Beating Hearts

Quantification of the tricuspid valve (TV) leaflets mechanical strain is important in order to understand valve pathophysiology and to develop effective treatment strategies. Many of the traditional methods used to dynamically open and close the cardiac valves in vitro via flow simulators require valve dissection. Recent studies, however, have shown that restriction of the atrioventricular valve annuli could significantly change their in vivo deformation. For the first time, the porcine valve leaflets deformation was measured in a passive ex vivo beating heart without isolating and remounting the valve annuli. In particular, the right ventricular apexes of porcine hearts ($n=8$) were connected to a pulse-duplicator pump that maintained a pulsatile flow from and to a reservoir connected to the right atrium and the pulmonary arteries. This pump provided a right ventricular pressure (RVP) waveform that closely matched physiological values, leading to opening and closure of the tricuspid and pulmonary valves (PVs). At the midsection of the valve leaflets, the peak areal strain was $9.8 \pm 2.0\%$ (mean \pm standard error). The peak strain was $5.6 \pm 1.1\%$ and $4.3 \pm 1.0\%$ in the circumferential and radial directions, respectively. Although the right ventricle was beating passively, the leaflet peak areal strains closely matched the values measured in other atrioventricular valves (i.e., the mitral valve (MV)) in vivo. This technique can be used to measure leaflet strains with and without the presence of valve lesions to help develop/evaluate treatment strategies to restore normal valve deformation. [DOI: 10.1115/1.4034621]

Introduction

As a one-way valve, the tricuspid valve (TV) guides the blood from the right atrium to the right ventricle during the atrial systole and prevents its backflow during the ventricular systole [1]. During the process of valve closure, its leaflets undergo complicated dynamic deformation and loadings. Quantification of such dynamic deformations is important because the development of treatment strategies for TV dysfunctions relies on a comprehensive understanding of its normal biomechanical environment. Among TV dysfunctions, TV regurgitation is one of the most common ones, which in most cases requires TV repair or total valve replacement [2,3]. The pathophysiology of TV regurgitation is closely related to the dynamic deformation of the valve annulus and leaflet coaptation [4]. Accurate quantification of normal biomechanical behavior of the TV leaflets during the cardiac cycle is essential for the development and evaluation of successful/efficient repair strategies and/or prosthetic valves that aim to mimic native valves.

A large group of researchers have studied the biomechanical behavior and dynamic deformations of the mitral valve (MV) [5–12], the atrioventricular valve analogous to the TV on the left

heart. There are also a few studies that focus on TV geometry and annulus deformation [13–15]. While these studies are extremely important, they provide no information about the dynamic mechanical strains of the TV leaflets. In terms of experimental techniques, the previous valvular studies can be categorized into two main groups: in vivo studies [5–7,9–11,13–15] and in vitro studies [12,16,17]. In vivo ovine and porcine studies are frequently used as excellent models prior to clinical studies [6,7,9]. Such studies, however, require surgical operating rooms and animal care facilities, which are often costly and should be used only prior to clinical approaches. In vitro studies, while less costly, were previously only conducted on excised valves [12,16]. In these studies, the excised valves are generally mounted on a prosthetic rigid annulus and subjected to pulsatile pressure in a flow simulator. The outcome of such studies is limited since it has been shown that the cardiac valve annulus is dynamically deforming during the cardiac cycle [9] and, thus, valve annulus restriction could significantly alter the leaflet strains [6].

Recently, an ex vivo approach using the entire porcine heart (instead of using isolated valves) has been developed to image valve motion and to study hemodynamics in the left chambers of the heart [18]. In the present study, we have used a modified ex vivo apparatus to open and close cardiac valves in the right side of the heart passively. In particular, for the first time, we have been able to visualize the dynamic deformations of the TV and measure the mechanical strains on the septal leaflet. Our method has

¹Corresponding author.

Manuscript received May 22, 2016; final manuscript received August 23, 2016; published online October 21, 2016. Assoc. Editor: Jessica E. Wagenseil.

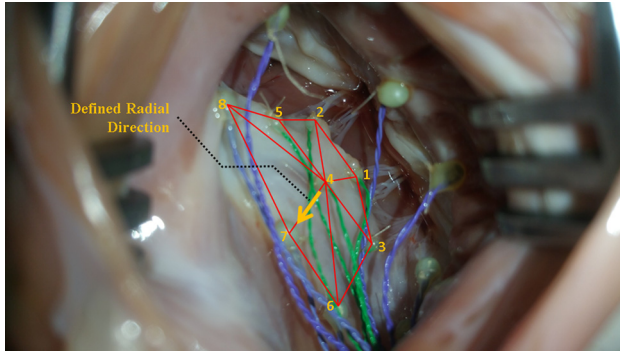


Fig. 4 Crystals are numbered on the leaflet. The straight lines connecting the numbered crystals show the triangular elements used for strain calculation. The radial direction was defined by a vector connecting crystal 4 to crystal 7.

straight barbed hose fitting connected to the right ventricle. A modified Luer Lok connector with a long tail was used to provide a safe passage for the pressure probe through the T-shaped pipe fitting as it was inserted into the ventricular chamber (Fig. 2). To allow one to visualize the leaflet motion, a backup seal followed by a dome valve was assembled inside the T-shaped pipe fitting before the Luer Lok assembly. As such, at any point during the experiment, we were able to remove the Luer Lok assembly and insert an endoscopic camera without causing any leaks. The same assembly was used to connect the pressure transducer to the superior vena cava and pulmonary artery as well. The inferior vena cava and other critical vessels were sealed using umbilical clamps to prevent leaks (Fig. 3). Cable ties or worm-drive clamps were used at the other connections to prevent leaks. Flexible $\frac{3}{4}$ -in. PVC tubes were used for all the tubing, and the connections and fittings were selected accordingly.

Sample Preparation. Fresh porcine hearts were obtained from a local slaughterhouse (3-D Meats, Dalton, OH) and were transported to our laboratory (in approximately 40 min) while submerged in isotonic phosphate buffered saline (PBS) and covered with ice immediately after the animals were slaughtered. The hearts were flushed using PBS to remove blood clots. In order to measure positional data, a total of 16 sonocrystals (Sonometrics Co., London, ON, Canada) were sutured to the valve annulus, septal leaflets, and myocardium (Fig. 4). To prevent any damage to the hearts, the sonocrystal wires were passed into the ventricle

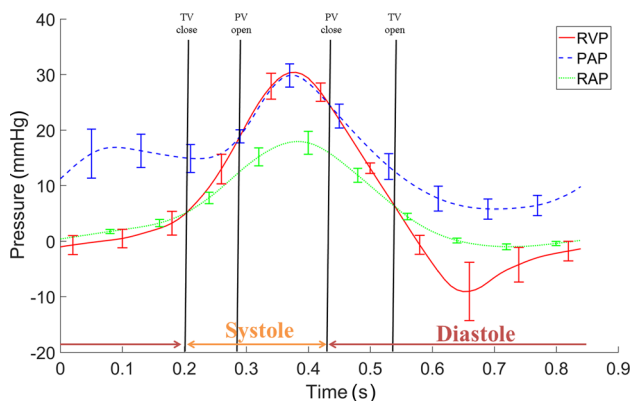


Fig. 5 Right heart pressure during the cardiac cycle averaged over all of the hearts. The bars are standard errors ($n = 8$). The vertical lines show the opening and closure of the pulmonary valve (PV) and tricuspid valve (TV): TV closed at 0.2s and opened at 0.54s; the pulmonary valve opened at 0.29s and closed at 0.44s.

through the inferior vena cava and the suturing process was conducted via the superior vena cava. As shown in Fig. 4, two crystals (1 mm) were sutured close to the edge, three (1 mm) at the mid-section, and three (2 mm) close to the annulus on the septal leaflet. Five more crystals (2 mm) were sutured around the annulus. In addition, three crystals (3 mm) were connected outside of the heart close to the apex in order to define the reference frame for positional measurements. All crystal wires were passed through the inferior vena cava. PBS with pH of 7.4 was used as the circulation fluid to help prevent the myocardium, especially the endocardium, from degenerating rapidly. During preparation and data collection, samples were submerged in PBS and/or PBS was sprayed on the surfaces exposed to the air to prevent drying. The sonocrystals were connected to the sonomicrometer device (TRX Series 16, Sonometrics Co., London, ON, Canada) to acquire the positional data. The pressure and flow signals were sent to the sonomicrometer as well as a data acquisition card (6036E, National Instruments, Austin, TX) directly connected to the computer. The pump controller provided a standard 70 bpm waveform which was used in the experiment. This waveform complied with the requirements of the International Standard Organization (ISO 5840) and U.S. Food and Drug Administration guidelines for heart valve testing [24]. After stabilization of the flow rate and periodic pressure signals, the sonomicrometer potentiometers were adjusted to maximize signal-to-noise ratio. Finally, an endoscopic camera (SSVR-710 Snakescope) was inserted into the heart to visualize the leaflet motion and ensure that the leaflets were coapting properly. The data acquisition was then initiated with a rate of 100 Hz (according to ISO 5840 requirements) and for a period of 20 s (2000 data points). Eight hearts were tested using the aforementioned procedure.

Strain Calculation. SonoSOFT (Sonometrics Co., London, ON, Canada) software was used to modify the recorded displacement and pressure signals. SonoXYZ (Sonometrics Co., London, ON, Canada) software was used to calculate the positional coordinates of the crystals during each cardiac cycle with respect to a defined coordinate system. These positional data were used to calculate the strain tensor based on a previously used method [6,25,26]. The triangulation was done manually according to pattern shown in Fig. 4. Since only eight crystals were sutured on the septal leaflet (the remaining eight crystals were sutured on the annulus and outside of the heart, as stated previously), their positioning was the same for all eight hearts and no automated triangulation was necessary.

After calculating the crystal positional data from the recorded raw data, the positional data were averaged over the 22 recorded beats for all crystals in each heart. The average positional data were then used to calculate the strains and stretches using the method explained in the Appendix section.

Pressures Data Analysis. The sonomicrometer data acquisition system was used to obtain both pressure and displacement signals. No synchronization process was necessary as the data were already synchronized for each node and heart. During all of the experiments, the signals of the right atrial pressure (RAP), RVP, and pulmonary artery pressure (PAP) were monitored and recorded. Before using such data, however, a few pressure corrections were conducted in the signals from each heart. The first correction was made to adjust the zero level. In particular, for each heart, there was a height difference between the free surface of the fluid in the reservoir and the right atrium. To remove the hydrostatic pressure magnitude in the measurement, the height was measured for each heart and the equivalent hydrostatic pressure was subtracted from the pressure signals. As a result, the minimum of the RVP and RAP shifted to a level close to zero. In addition, as the hearts were assembled vertically, there was a height difference between the bottom of the ventricle and the pulmonary artery where the pressure sensors were positioned to

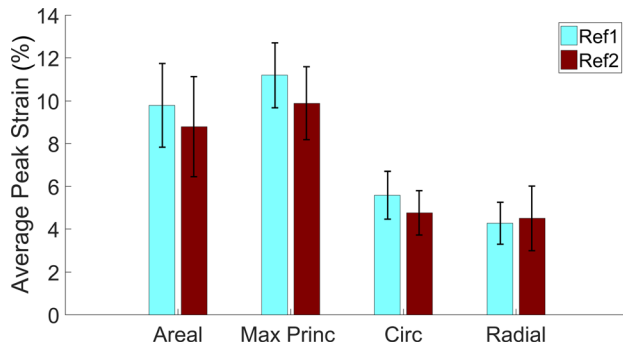


Fig. 6 Average peak areal, maximum principal (Max Princ), circumferential (Circ), and radial strains at the leaflet midpoint measured with respect to reference 1 (Ref1, minimum RAP) and reference 2 (Ref2, end diastole). The error bars are standard error ($n = 8$).

measure RVP and PAP, respectively. This height difference was also measured for each heart, and the equivalent hydrostatic pressure was subtracted from the PAP. Although these heights and their equivalent hydrostatic pressures were small, this correction process was necessary to obtain a consistent and comparable cardiac pressure graph for all experiments. In all eight experiments, the recorded pressures and positional data were averaged over all the 22 recorded beats.

Results

Pressure. As shown in Fig. 5, although the porcine hearts were passively beating, the recorded pressure compared well with

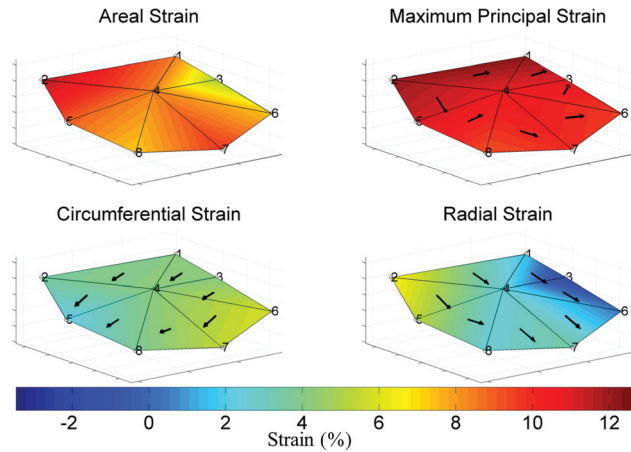


Fig. 8 The areal, maximum principal, circumferential, and radial strains at maximum RVP. The strains are averaged over all the hearts ($n = 8$) and are presented on a typical septal leaflet. Minimum RAP is used as the reference for strain calculation. The arrows are showing the direction of the strains at the center of each triangular surface.

in vivo human cardiac pressures [27]. The small standard errors show that despite the variability among the porcine samples, the pressures for each heart do not deviate much from the average value for the eight hearts. The measured RVP ranged from values close to zero up to approximately 30 mm Hg, similar to the reported porcine values (2 – 33 mm Hg [28–31]). The measured PAP ranged from approximately 6 to 30 mm Hg. The RAP remained relatively close to zero during diastole. We were not

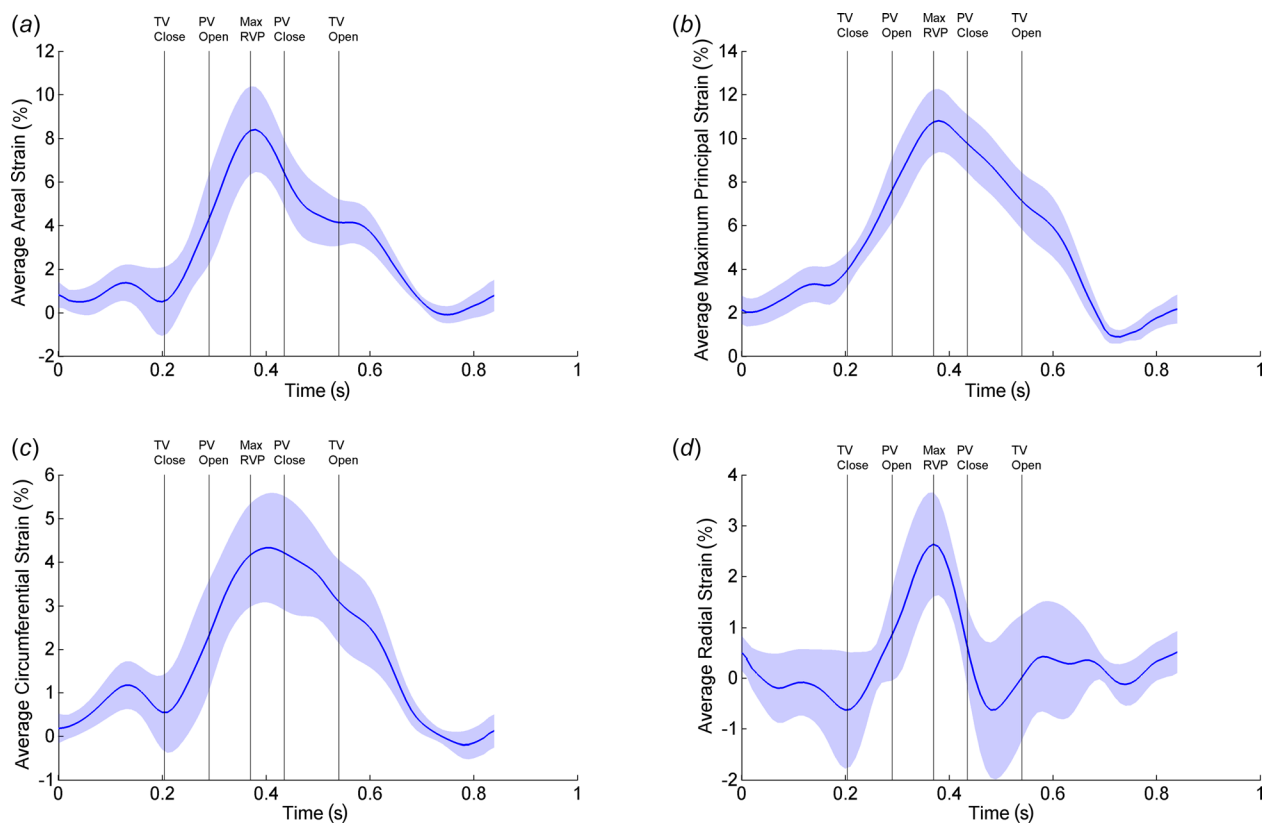


Fig. 7 The temporal strain variations during the cardiac cycle. (a) The areal, (b) maximum principal, (c) circumferential, and (d) radial strains at the leaflet midpoint averaged over all of the hearts. The shaded area shows the standard error ($n = 8$). Vertical lines show the time points for TV closing, PV opening, maximum RVP, PV closing, and TV opening, respectively, from left to right.

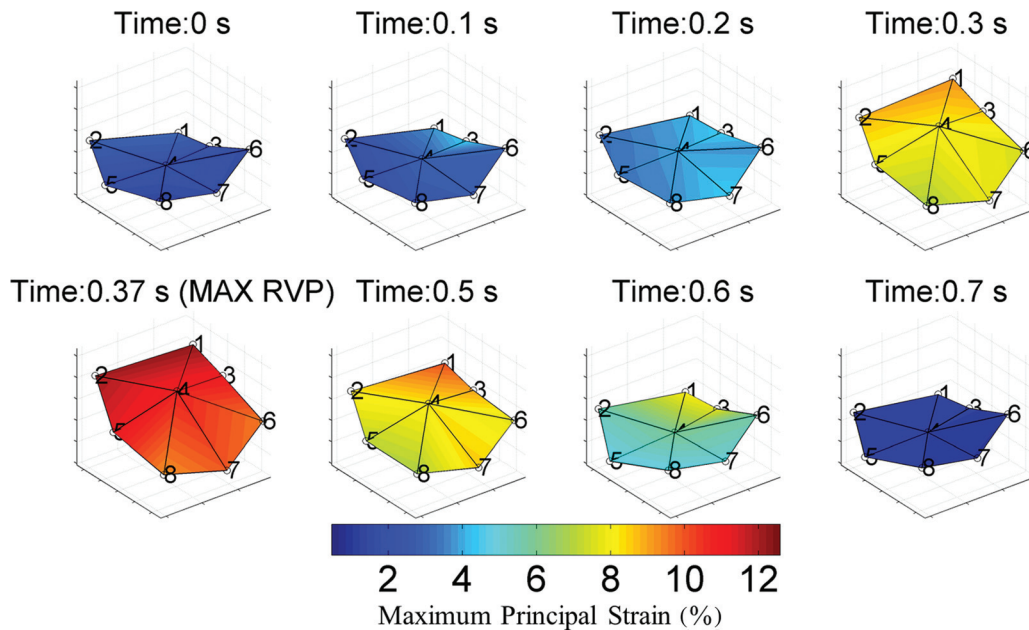


Fig. 9 Distribution of the maximum principal strain over the leaflet during the septal entire cardiac cycle. Maximum principal strain is averaged over all of the hearts ($n = 8$) and showed over a typical septal leaflet during the cardiac cycle.

able to find reliable PAP and RAP values for porcine hearts in the literature, but the measured values for these two signals (Fig. 5) were comparable to those of a human [27]. The RVP average signal also shows a small drop right at the beginning of the diastole. A closer examination of the RVP signal in Fig. 5 shows that the TV closes at approximately 0.2 s, where the RVP intersects with the RAP; the pulmonary artery valve (PV) opens at 0.29 s, where the RVP meets the PAP; the PV closes approximately at 0.44 s, where the RVP separates from the PAP; and finally, the TV opens approximately at 0.54 s, where the RVP crosses the RAP once more. The average flow rate for all the hearts was 2.63 ± 0.13 l/min.

Deformation. The position of the fiducial markers at the minimum left ventricular pressure has been previously used as the referential configuration for calculating the strains and stretches in the left heart [5,7]. As such, it was a reasonable assumption to use the minimum RVP as the referential (undeformed) configuration in our study as well. However, as discussed above, there existed a small drop in the measured RVP signal. Since in a normal cardiac cycle, RVP and RAP approximately overlap during the diastole [27], their minimum should occur at the same place in this part of the cardiac cycle. Therefore, one of the reference configurations was chosen to reflect the nodal positions at the minimum RAP. The other reference configuration was chosen to represent the positional data at the end-diastole, which has also been used in similar studies [5]. Figure 6 shows the calculated peak areal strain, maximum principal strain, circumferential strain, and radial strain at the center point of the leaflet (point number 4) averaged for all eight hearts using the two aforementioned references. Figure 6 also shows the strain standard errors for the eight hearts. There was no significant difference between the strains measured using two different reference configurations ($p > 0.14$ in all cases, paired student t-test). The same observation has been reported for the mitral valve anterior leaflet [5]. As shown in Fig. 6, the peak areal strain (9.8%) and the peak maximum principal strain (11.2%) were significantly different ($p < 0.008$ in all cases, paired student t-test) from the peak circumferential strain (5.6%) and the peak radial strain (4.3%). However, there was no significant difference ($p \approx 0.24$, paired student t-test) between the peak

circumferential and the peak radial strains (the numbers quantified using minimum RAP as the undeformed reference (Ref1 in Fig. 6)).

Figure 7 shows the temporal strain variations over a cardiac cycle. The strain values were averaged at the leaflet midpoint for the eight hearts at each time point. The leaflets experienced positive strain for the majority of the time points during the cardiac cycle. Comparing the strain graphs with the pressure graph shows that immediately after the TV closed ($t = 0.2$ s), all the quantified strains rose rapidly and reached their peaks' values at the maximum RVP ($t \approx 0.4$ s). The strains subsequently dropped, reaching their minimum values at $t \approx 0.65$ s, with the exception of the radial strain, which reached the minimum value at $t \approx 0.5$ s. Overall, the strain values were extremely small during diastole and increased during systole. Note that the peak of the means (Fig. 6) is always less than (or ideally equal to) the mean of the peaks (Fig. 7), since the maximum values of the signals for each heart do not necessarily happen exactly at the same time.

Figure 8 shows the spatial distribution of the strains over the leaflet at the maximum RVP. At this pressure level, the strains were averaged over all eight hearts. The averaged data are illustrated for a typical septal leaflet. As shown in Fig. 8, the maximum principal strain is distributed uniformly over the leaflet at maximum RVP, while the areal strain is not as uniform. There is much heterogeneity in the spatial distribution of the circumferential strain and radial strain over the septal leaflet. While higher values for circumferential strain were observed toward the posterior of the leaflet, the radial strains reached higher values in areas near the anterior.

Figure 9 shows the distribution of the maximum principal strains across the leaflet over the entire cardiac cycle. The maximum principal strains were averaged for the eight hearts. Similar to Fig. 8, the averaged data in Fig. 9 are also illustrated over a typical septal leaflet; in this figure, the strain data are presented over different time points of the cardiac cycle. The maximum principal strain was uniformly distributed over the leaflet for nearly the entire cardiac cycle. The distribution of the areal, maximum principal, circumferential, and radial strains across the leaflet over the entire cardiac cycle is provided in the Supplementary Material, which are available under the "Supplemental Materials" tab for this paper on the ASME Digital Collection.

Discussion

Our novel *ex vivo* beating heart apparatus was able to produce repeatable data with high temporal resolution. Using our passive beating heart, we were able to reproduce ventricular pressure waves that matched the physiological values of an active heart [27]. Porcine hearts are excellent models for valve studies and pressure values at the pulmonary side are similar in human and porcine hearts. In particular, human RVP ranges approximately from 0 to 30 mm Hg [27,32] and porcine RVP ranges roughly from 0 up to around 33 mm Hg [28–31]. Such a similarity also exists in the left side of the heart [1,33].

To the best of our knowledge, the *in vivo* strains in porcine tricuspid valve leaflets have not yet been quantified. Thus, it is not possible to compare our deformation results with *in vivo* TV deformation values. The average values of the maximum principal strains and the areal strains quantified at maximum RVP in our *ex vivo* apparatus were 11.2% and 9.8%, respectively. These values compared well with those calculated in the ovine mitral valve (MV) anterior leaflet (12.3% and 12.7% for the areal strain and the maximum principal strain, respectively [5]). Such a similarity in the strain values is of particular interest, as it shows that while the two leaflets are subjected to different levels of ventricular pressures, they deform in a relatively similar manner.

As stated in the results section, the RAP was slightly greater than the expected values during systole (in comparison to human RAP profiles). Aside from potential differences in human and porcine hearts, such a discrepancy could be due to slight TV regurgitations during systole, causing the pressure in the ventricle to go higher than the normal values. The probable reason for this regurgitation could be the weight of the crystals (~2–3 mg per each 1-mm crystal and ~15–20 mg per each 2-mm crystal) on the septal leaflet. In addition, the crystal wires could have resisted the necessary bending deformation and prevented the full closure of the valve. Although a slight leak from the TV during the experiments was possible, the endoscopic monitoring did not show any gap between the leaflets, and the leaflet coaptation was visually confirmed in all cases (see the videos which are available under the “Supplemental Materials” tab for this paper on the ASME Digital Collection). We also observed a small drop in the RVP average signal at the beginning of the diastole. When the pump finished the systolic step, the fluid was immediately sucked into the heart chambers, causing a drop in the pressure at the bottom of the ventricle where the pressure sensor was placed. Finally, a small bump in PAP can be seen at approximately 0.1 s, indicating a slight back flow after the pulmonary valve closed. In our setup, after connecting the straight barbed hose fitting to the heart, approximately 3 cm of the pulmonary artery was free to expand and a degree of physiological damping was present. However, a large portion of the pulmonary artery was used to obtain a sealed connection to the hydraulic circuit, and the compliance was not enough to dampen the changes in the pressure. A well-tuned compliance chamber might be useful for eliminating this inertial effect in the PAP signal. It should be noted that fluid height in the backflow tube going into the reservoir was monitored, and a valve positioned between the pulmonary artery and the reservoir was used to adjust the pressure; however, complete damping of the inertial effect would have required the addition of a compliance chamber. In this study, we did not choose to use a well-tuned compliance chamber as we made a compromise to ensure the tissue was as fresh as possible, saving time by not adding any additional components.

Unlike the MV leaflets, in which significant differences exist between the maximum strain in the circumferential and radial directions [5,6,16], no significant difference existed between circumferential and radial strains in the TV septal leaflet at the maximum RVP. A potential explanation is that the TV septal leaflet has a more isotropic extracellular matrix microstructural architecture in comparison to the MV anterior and posterior leaflets. The anisotropic nature of the MV anterior leaflet has been demonstrated previously [34]. Biaxial mechanical testing and

measurement of tissue microstructural architecture (e.g., via small angle light scattering) could identify the degree of anisotropy in TV septal leaflets. Due to the fact that the number of channels available for sonomicrometry crystals was limited to 16, we were not able to measure the deformation of the TV anterior and posterior leaflets to make such a comparison among the *ex vivo* strain values. Further research is required to quantify strain values in the TV anterior and posterior leaflets in the future [35,36].

There are many advantages in using porcine hearts in our experiment, as fresh tissues can be obtained and the biomechanical behavior of the valves is less affected by the activity of degenerative enzymes in the extracellular matrix. In addition, in comparison to human cadaverous tissues, younger porcine samples with less variability are available [34]. However, one should always be cautious in drawing conclusions regarding human tissue responses based solely on animal studies [37]. The advantage of our *ex vivo* apparatus is that, if necessary, human cadaverous tissues can be used in conducting similar experiments without any additional complications.

Sonomicrometry crystals may affect the measured deformations in different ways. The process of attaching the crystals to the leaflet may cause some localized and permanent changes to the leaflet structural properties. Although these changes were not measurable in our setup, much caution was used to prevent damage to the tissue during the suturing process. It is noteworthy that these changes were presumably restricted to the immediate vicinity of the crystal. As per potential of error due to buoyancy and/or inertia, the piezocrystals had same density as that of water or tissue. In addition, the crystals were extremely small compared to the size of their surrounding tissues. Therefore, their interference with natural leaflet motion was minimal. Crystals, of course, were connected to the sonomicrometer instrument via wires. One may consider the tethering effects of these connecting wires as a potential source for leaflet motion restriction. The crystals were connected to sonomicrometer using 38-gauge copper wires, which were flexible. In order for the crystal wires to alter the natural motion of the leaflets in any way, the wires should have been tethered close to the leaflet surface, with little or no out-of-plane slack. As such, we made sure that the wires had enough slack and the natural motion of the leaflets was not restricted. Despite its few limitations, sonomicrometry have been used extensively in the valve studies [6,7,9,14,38–40].

A major limitation of our experiment is the *passive* nature of the beating heart. The contraction of papillary muscles and the activation of ventricular and atrial muscles potentially change the loading condition on the leaflet annulus and chordae tendineae. Although the *ex vivo* passive beating heart is not identical to the *in vivo* active hearts, unlike the *in vitro* studies of the excised cardiac valves [12,16,17], the TV annulus is not restricted in the *ex vivo* apparatus. *in vivo* studies of the TV motion have shown that TV annulus size dynamically changes during the normal cardiac cycle [14]. The *ex vivo* beating heart at least maintains the passive component of such deformation in the TV annulus. In short, even though the *ex vivo* beating heart experiment is not identical to the *in vivo* heart, it is more realistic than the isolated valve experiments when it comes to the valve annulus deformation.

There exists a major advantage in using a passive beating heart in the verification of combined valve and ventricle computational models [41]. In particular, because the cardiac muscles are not active and the ventricular pressure is the only load applied to the cardiac tissues, one could use the *ex vivo* beating heart to validate combined valve and ventricle models absent the active stress components of the cardiac tissues. In addition to detailed pressure and strain measurements, the entire heart can be imaged and segmented following the experiment to provide a subject-specific computational model.

Although our study was conducted using PBS, there is no limitation in using other nonclear fluids in our apparatus, as our strain measurement does not rely on visual access to the valves. Such a capability is of great importance because recent studies have

shown that the flow properties (particularly the transition to turbulence) could be significantly different in blood in comparison to optically clear viscosity-matched blood substitutes [42]. Since the transition to turbulence could happen in the proximity of the cardiac valves, measurements of valve deformation using blood should be conducted in the future.

In summary, we developed an experimental setup to measure the dynamic deformation of the porcine TV septal leaflets. We observed that the leaflet strain values are similar to those measured in vivo in leaflets of the other atrioventricular valve (i.e., the mitral valve). In future studies, our experimental model can be used to evaluate mechanical strains on different TV leaflets. In addition, our experimental setup can be beneficial in studying primary valve lesions such as chordae rupture, secondary valve lesions such as pulmonary hypertension, and valve repair procedures such as ring annuloplasty and/or leaflet resection.

Acknowledgment

The authors would like to thank Anthony Black for his assistance during the experimental process. Provision of the porcine hearts from 3-D Meats (Dalton, OH) and technical consultation from Devesh Amaty, Gus Kalogeros, and Wayne Smith are also acknowledged. Funding for this project was provided in part by the Firestone Research Initiative Fellowship Award and by American Heart Association Grant No. 16SDG27770088.

Nomenclature

- \mathbf{e} = Eulerian strain tensor
- e_{areal} = areal change
- e_{cir} = circumferential strain
- \mathbf{e}_i = orthogonal unit vectors
- e_{ij} = components of the Eulerian strain tensor
- e_{max} = max principal strain
- e_{rad} = radial strain
- g = square value of the scaling factor in the current (deformed) configuration
- \mathbf{g}_i = covariant base vectors in the current (deformed) configuration
- g_{ij} = components of the deformed metric tensor
- \mathbf{G}_i = covariant base vectors in the referential (undeformed) configuration
- G_{ij} = components of the undeformed metric tensor
- \mathbf{g} = contravariant base vectors in the current (deformed) configuration
- i, j = dummy indices
- p = p -value of paired student t-test
- \mathbf{p} = position vector in the current (deformed) configuration
- \mathbf{P} = position vector in the referential (undeformed) configuration
- $\hat{\mathbf{p}}$ = position vector of a node in the current (deformed) configuration
- $\hat{\mathbf{P}}$ = position vector of a node in the referential (undeformed) configuration
- t = time
- \mathbf{V}_{cir} = circumferential direction vector in the triangular element plane
- \mathbf{V}_{max} = direction of the maximum principal strain
- \mathbf{V}_{rad} = radial direction vector in the triangular element plane
- x^j = current (spatial) coordinates
- X^i = reference (material) coordinates
- $_{,\alpha}$ = derivative with respect to X^α ($\partial/\partial X^\alpha$)
- α, β = dummy indices (taking values 1 and 2)
- η = computational domain coordinate
- ξ = computational domain coordinate
- ω = bilinear basis function

Abbreviations

MV = mitral valve

PAP = pulmonary artery pressure
 PBS = phosphate buffered saline
 PV = pulmonary valve
 RAP = right atrial pressure
 RVP = right ventricular pressure
 TV = tricuspid valve

Appendix

The initial and current positions of the crystals, which will be referred to as nodes from this point forward, are represented by $\hat{\mathbf{P}}$ and $\hat{\mathbf{p}}$, respectively. The position vector of each point on the surface of each triangular element is defined by the bilinear interpolation of the nodal elements of the triangle

$$\mathbf{P} = \sum_{i=1}^3 \omega_i(\xi, \eta) \hat{\mathbf{P}}_i \quad (\text{A1})$$

$$\mathbf{p} = \sum_{i=1}^3 \omega_i(\xi, \eta) \hat{\mathbf{p}}_i \quad (\text{A2})$$

where $\omega_i(\xi, \eta)$ are the bilinear basis functions and ξ ($\in [0, 1]$) and η ($\in [0, 1]$) are the computational domain coordinates.

During the deformation, X^i represented the reference (material) coordinates and x^j represented the current (spatial) coordinates. The deformed coordinate was defined as a function of the reference coordinate $x^i = x^i(X^i)$, where $i = 1, 2$, and 3; assuming that $X^3 = X^3(X^1, X^2)$, x^i was rewritten as $x^i = x^i(X^1, X^2)$ [26]. Therefore, the position vector of a point at the reference configuration and that of the current configuration is written as

$$\mathbf{P} = X^\alpha \mathbf{e}_\alpha + X^3(X^1, X^2) \mathbf{e}_3 \quad (\text{A3})$$

$$\mathbf{p} = x^\alpha(X^1, X^2) \mathbf{e}_\alpha + x^3(X^1, X^2) \mathbf{e}_3 \quad (\text{A4})$$

where α takes values of 1 and 2 and the summation convention on repeated indices is implied; \mathbf{e}_i represents an orthogonal coordinate system. The covariant base vectors in undeformed and deformed configurations are

$$\mathbf{G}_\alpha = \mathbf{P}_{,\alpha} = \mathbf{e}_\alpha + X^3_{,\alpha} \mathbf{e}_3 \quad (\text{A5})$$

$$\mathbf{g}_\alpha = \mathbf{p}_{,\alpha} = x^\beta_{,\alpha} \mathbf{e}_\beta + x^3_{,\alpha} \mathbf{e}_3 \quad (\text{A6})$$

where α and β take values of 1 and 2 and the summation convention on repeated indices is implied; $_{,\alpha}$ denotes derivative with respect to X^α ($\partial/\partial X^\alpha$). The third covariant base vectors \mathbf{G}_3 and \mathbf{g}_3 were calculated as described previously [25]

$$\mathbf{G}_3 = \frac{\mathbf{G}_1 \times \mathbf{G}_2}{\|\mathbf{G}_1 \times \mathbf{G}_2\|} \quad (\text{A7})$$

$$\mathbf{g}_3 = \frac{\mathbf{g}_1 \times \mathbf{g}_2}{\|\mathbf{g}_1 \times \mathbf{g}_2\|} \quad (\text{A8})$$

The components of the undeformed metric tensors G_{ij} and the deformed metric tensor g_{ij} were calculated using the covariant base vectors in the referential and current configurations. The elements of the metric tensors are

$$G_{ij} = \mathbf{G}_i \cdot \mathbf{G}_j \quad (\text{A9})$$

$$g_{ij} = \mathbf{g}_i \cdot \mathbf{g}_j \quad (\text{A10})$$

Consistent with other valve studies, we chose the Eulerian strain as the main measure of deformation in our calculation [5,7]. The components of Eulerian strain were calculated using

$$e_{ij} = \frac{g_{ij} - G_{ij}}{2} \quad (A11)$$

where the Eulerian strain tensor is $\mathbf{e} = e_{ij}\mathbf{g}^i\mathbf{g}^j$ and the contravariant base vectors in the deformed configuration are defined by

$$\mathbf{g}^1 = \frac{\mathbf{g}_2 \times \mathbf{g}_3}{\sqrt{g}} \quad (A12)$$

$$\mathbf{g}^2 = \frac{\mathbf{g}_3 \times \mathbf{g}_1}{\sqrt{g}} \quad (A13)$$

$$\mathbf{g}^3 = \frac{\mathbf{g}_1 \times \mathbf{g}_2}{\sqrt{g}} \quad (A14)$$

where

$$\sqrt{g} = \mathbf{g}_1 \cdot (\mathbf{g}_2 \times \mathbf{g}_3) \quad (A15)$$

The maximum strain e_{\max} and its direction \mathbf{V}_{\max} were calculated by solving the eigenvalue problem for the Eulerian strain tensor. As shown in Fig. 4, the vector from crystal 4 to crystal 7 was chosen as the global radial direction. To calculate the radial and circumferential directions for each triangular element, the normal vector to the element was calculated using the cross product of two side vectors of the element. The cross product of the normal vector with the global radial direction vector provided the circumferential direction vector \mathbf{V}_{cir} in the triangular element plane; the cross product of the normal vector with the local circumferential direction vector provided the local radial direction vector \mathbf{V}_{rad} in the triangular element plan. The circumferential and radial strains were then calculated

$$e_{\text{cir}} = \mathbf{V}_{\text{cir}} \cdot \mathbf{e} \cdot \mathbf{V}_{\text{cir}} \quad (A16)$$

$$e_{\text{rad}} = \mathbf{V}_{\text{rad}} \cdot \mathbf{e} \cdot \mathbf{V}_{\text{rad}} \quad (A17)$$

where e_{cir} and e_{rad} were circumferential and radial strains, respectively.

Finally, using the Eulerian strain definition, the areal strain was calculated as

$$e_{\text{areal}} = 1 - \frac{1}{\lambda_{\text{areal}}} \quad (A18)$$

where λ_{areal} , the areal change, was given by

$$\lambda_{\text{areal}} = \sqrt{\frac{\det(g_{ij})}{\det(G_{ij})}} \quad (A19)$$

References

- Hall, J. E., 2010, *Guyton and Hall Textbook of Medical Physiology*, Elsevier Health Sciences, Philadelphia, PA.
- Vassileva, C. M., Shabosky, J., Boley, T., Maxwell, S., and Hazelrigg, S., 2012, "Tricuspid Valve Surgery: The Past 10 Years From the Nationwide Inpatient Sample (NIS) Database," *J. Thorac. Cardiovasc. Surg.*, **143**(5), pp. 1043–1049.
- Guenther, T., Noebauer, C., Mazzitelli, D., Busch, R., Tassani-Prell, P., and Lange, R., 2008, "Tricuspid Valve Surgery: A Thirty-Year Assessment of Early and Late Outcome," *Eur. J. Cardio-Thorac. Surg.*, **34**(2), pp. 402–409.
- Come, P. C., and Riley, M. F., 1985, "Tricuspid Annular Dilatation and Failure of Tricuspid Leaflet Coaptation in Tricuspid Regurgitation," *Am. J. Cardiol.*, **55**(5), pp. 599–601.
- Rausch, M. K., Bothe, W., Kvitting, J. E., Göktepe, S., Miller, D. C., and Kuhl, E., 2011, "In Vivo Dynamic Strains of the Ovine Anterior Mitral Valve Leaflet," *J. Biomech.*, **44**(6), pp. 1149–1157.
- Amini, R., Eckert, C. E., Koomalsingh, K., McGarvey, J., Minakawa, M., Gorman, J. H., Gorman, R. C., and Sacks, M. S., 2012, "On the In Vivo Deformation of the Mitral Valve Anterior Leaflet: Effects of Annular Geometry and Referential Configuration," *Ann. Biomed. Eng.*, **40**(7), pp. 1455–1467.
- Sacks, M. S., Enomoto, Y., Graybill, J. R., Merryman, W. D., Zeeshan, A., Yoganathan, A. P., Levy, R. J., Gorman, R. C., and Gorman, J. H., 2006, "In-Vivo Dynamic Deformation of the Mitral Valve Anterior Leaflet," *Ann. Thorac. Surg.*, **82**(4), pp. 1369–1377.
- Sacks, M. S., Merryman, W. D., and Schmidt, D. E., 2009, "On the Biomechanics of Heart Valve Function," *J. Biomech.*, **42**(12), pp. 1804–1824.
- Eckert, C. E., Zubiate, B., Vergnat, M., Gorman, J. H., III, Gorman, R. C., and Sacks, M. S., 2009, "In Vivo Dynamic Deformation of the Mitral Valve Annulus," *Ann. Biomed. Eng.*, **37**(9), pp. 1757–1771.
- Krishnamurthy, G., Itoh, A., Bothe, W., Swanson, J. C., Kuhl, E., Karlsson, M., Miller, D. C., and Ingels, N. B., 2009, "Stress-Strain Behavior of Mitral Valve Leaflets in the Beating Ovine Heart," *J. Biomech.*, **42**(12), pp. 1909–1916.
- Krishnamurthy, G., Itoh, A., Swanson, J. C., Bothe, W., Karlsson, M., Kuhl, E., Miller, D. C., and Ingels, N. B., 2009, "Regional Stiffening of the Mitral Valve Anterior Leaflet in the Beating Ovine Heart," *J. Biomech.*, **42**(16), pp. 2697–2701.
- Sacks, M. S., He, Z., Baijens, L., Wanant, S., Shah, P., Sugimoto, H., and Yoganathan, A. P., 2002, "Surface Strains in the Anterior Leaflet of the Functioning Mitral Valve," *Ann. Biomed. Eng.*, **30**(10), pp. 1281–1290.
- Hiro, M. E., Jouan, J., Pagel, M. R., Lansac, E., Lim, K. H., Lim, H., and Duran, C. M., 2004, "Sonometric Study of the Normal Tricuspid Valve Annulus in Sheep," *J. Heart Valve Dis.*, **13**(3), pp. 452–460.
- Fawzy, H., Fukamachi, K., Mazer, C. D., Harrington, A., Latter, D., Bonneau, D., and Errett, L., 2011, "Complete Mapping of the Tricuspid Valve Apparatus Using Three-Dimensional Sonomicrometry," *J. Thorac. Cardiovasc. Surg.*, **141**(4), pp. 1037–1043.
- Jouan, J., Pagel, M. R., Hiro, M. E., Lim, K. H., Lansac, E., and Duran, C. M., 2007, "Further Information From a Sonometric Study of the Normal Tricuspid Valve Annulus in Sheep: Geometric Changes During the Cardiac Cycle," *J. Heart Valve Dis.*, **16**(5), pp. 511–518.
- He, Z., Ritchie, J., Grashow, J. S., Sacks, M. S., and Yoganathan, A. P., 2005, "In Vitro Dynamic Strain Behavior of the Mitral Valve Posterior Leaflet," *ASME J. Biomech. Eng.*, **127**(3), pp. 504–511.
- He, Z., Sacks, M. S., Baijens, L., Wanant, S., Shah, P., and Yoganathan, A. P., 2003, "Effects of Papillary Muscle Position on In-Vitro Dynamic Strain on the Porcine Mitral Valve," *J. Heart Valve Dis.*, **12**(4), pp. 488–494.
- Leopaldi, A., Vismara, R., Lemma, M., Valerio, L., Cervo, M., Mangini, A., Contino, M., Redaelli, A., Antona, C., and Fiore, G., 2012, "In Vitro Hemodynamics and Valve Imaging in Passive Beating Hearts," *J. Biomech.*, **45**(7), pp. 1133–1139.
- Chaudhury, R. A., Atlasman, V., Pathangey, G., Pracht, N., Adrian, R. J., and Frakes, D. H., 2016, "A High Performance Pulsatile Pump for Aortic Flow Experiments in 3-Dimensional Models," *Cardiovasc. Eng. Technol.*, **7**(2), pp. 1–11.
- Evin, M., Guivier-Curien, C., Pibarot, P., Kadem, L., and Rieu, R., 2016, "Are the Current Doppler Echocardiography Criteria Able to Discriminate Mitral Bileaflet Mechanical Heart Valve Malfunction? An In Vitro Study," *Artif. Organs*, **40**(5), pp. 52–60.
- Trawiński, Z., Wójcik, J., Nowicki, A., Olszewski, R., Balcerzak, A., Frankowska, E., Zegadlo, A., and Rydzynski, P., 2015, "Strain Examinations of the Left Ventricle Phantom by Ultrasound and Multislices Computed Tomography Imaging," *Biocybern. Biomed. Eng.*, **35**(4), pp. 255–263.
- Rahmani, B., Tzamtzis, S., Ghanbari, H., Burriesci, G., and Seifalian, A. M., 2012, "Manufacturing and Hydrodynamic Assessment of a Novel Aortic Valve Made of a New Nanocomposite Polymer," *J. Biomech.*, **45**(7), pp. 1205–1211.
- Cygan, S., Werys, K., Błaszczyk, Ł., Kubik, T., and Kałużynski, K., 2014, "Left Ventricle Phantom and Experimental Setup for MRI and Echocardiography—Preliminary Results of Data Acquisitions," *Biocybern. Biomed. Eng.*, **34**(1), pp. 19–24.
- Nolan, S. P., 1994, "The International Standard Cardiovascular Implants—Cardiac Valve Prostheses (ISO 5840:1989) and the FDA Draft Replacement Heart Valve Guidance (Version 4.0)," *J. Heart Valve Dis.*, **3**(4), pp. 347–349.
- Amini, R., Voycheck, C. A., and Debski, R. E., 2014, "A Method for Predicting Collagen Fiber Realignment in Non-Planar Tissue Surfaces as Applied to Glenohumeral Capsule During Clinically Relevant Deformation," *ASME J. Biomech. Eng.*, **136**(3), p. 031003.
- Filas, B. A., Knutsen, A. K., Bayly, P. V., and Taber, L. A., 2008, "A New Method for Measuring Deformation of Folding Surfaces During Morphogenesis," *ASME J. Biomech. Eng.*, **130**(6), p. 061010.
- Mohrman, D. E., and Heller, L. J., 2002, *Cardiovascular Physiology*, McGraw-Hill, New York.
- Greyson, C., Xu, Y., Cohen, J., and Schwartz, G. G., 1997, "Right Ventricular Dysfunction Persists Following Brief Right Ventricular Pressure Overload," *Cardiovasc. Res.*, **34**(2), pp. 281–288.
- Greyson, C., Xu, Y., Lu, L., and Schwartz, G. G., 2000, "Right Ventricular Pressure and Dilation During Pressure Overload Determine Dysfunction After Pressure Overload," *Am. J. Physiol.*, **278**(5), pp. H1414–1420.
- Schmitto, J. D., Doerge, H., Post, H., Coulibaly, M., Sellin, C., Popov, A. F., Sossalla, S., and Schoendube, F. A., 2009, "Progressive Right Ventricular Failure is Not Explained by Myocardial Ischemia in a Pig Model of Right Ventricular Pressure Overload," *Eur. J. Cardio-Thorac. Surg.*, **35**(2), pp. 229–234.
- Solomon, S. B., and Glantz, S. A., 1999, "Regional Ischemia Increases Sensitivity of Left Ventricular Relaxation to Volume in Pigs," *Am. J. Physiol.*, **276**(6 Pt 2), pp. H1994–2005.
- Redington, A. N., Gray, H. H., Hodson, M. E., Rigby, M. L., and Oldershaw, P. J., 1988, "Characterisation of the Normal Right Ventricular Pressure-Volume Relation by Biplane Angiography and Simultaneous Micromanometer Pressure Measurements," *Br. Heart J.*, **59**(1), pp. 23–30.

- [33] Hannon, J. P., Bossone, C. A., and Wade, C. E., 1990, "Normal Physiological Values for Conscious Pigs Used in Biomedical Research," *Lab. Anim. Sci.*, **40**(3), pp. 293–298.
- [34] May-Newman, K., and Yin, F. C., 1995, "Biaxial Mechanical Behavior of Excised Porcine Mitral Valve Leaflets," *Am. J. Physiol.*, **269**(4 Pt 2), pp. H1319–1327.
- [35] Billiar, K., and Sacks, M., 1997, "A Method to Quantify the Fiber Kinematics of Planar Tissues Under Biaxial Stretch," *J. Biomech.*, **30**(7), pp. 753–756.
- [36] Khoiy, K. A., and Amini, R., 2016, "On the Biaxial Mechanical Response of Porcine Tricuspid Valve Leaflets," *ASME J. Biomech. Eng.*, **138**(10), p. 104504.
- [37] Martin, C., and Sun, W., 2012, "Biomechanical Characterization of Aortic Valve Tissue in Humans and Common Animal Models," *J. Biomed. Mater. Res., Part A*, **100**(6), pp. 1591–1599.
- [38] Gorman, J. H., Jackson, B. M., Enomoto, Y., and Gorman, R. C., 2004, "The Effect of Regional Ischemia on Mitral Valve Annular Saddle Shape," *Ann. Thorac. Surg.*, **77**(2), pp. 544–548.
- [39] Gorman, J. H., Gorman, R. C., Jackson, B. M., Enomoto, Y., John-Sutton, M. G. S., and Edmunds, L. H., 2003, "Annuloplasty Ring Selection for Chronic Ischemic Mitral Regurgitation: Lessons From the Ovine Model," *Ann. Thorac. Surg.*, **76**(5), pp. 1556–1563.
- [40] Gorman, J. H., Gupta, K. B., Streicher, J. T., Gorman, R. C., Jackson, B. M., Ratcliffe, M. B., Bogen, D. K., and Edmunds, L. H., 1996, "Dynamic Three-Dimensional Imaging of the Mitral Valve and Left Ventricle by Rapid Sonomicrometry Array Localization," *J. Thorac. Cardiovasc. Surg.*, **112**(3), pp. 712–724.
- [41] Ge, L., Morrel, W. G., Ward, A., Mishra, R., Zhang, Z., Guccione, J. M., Grossi, E. A., and Ratcliffe, M. B., 2014, "Measurement of Mitral Leaflet and Annular Geometry and Stress After Repair of Posterior Leaflet Prolapse: Virtual Repair Using a Patient-Specific Finite Element Simulation," *Ann. Thorac. Surg.*, **97**(5), pp. 1496–1503.
- [42] Biswas, D., Casey, D., Crowder, D., Steinman, D. A., Yun, H. Y., and Loth, F., 2016, "Characterization of Transition to Turbulence for Blood in a Straight Pipe Under Steady Flow Conditions," *ASME J. Biomech. Eng.*, **138**(7), p. 071001.